

Cross-field demagnetization of stacks of tapes: 3D modelling and measurements

M. Kapolka¹, E. Pardo^{1a}, F. Grilli², A. Baskys^{3,4}, V. Climente-Alarcon³, B. A. Glowacki³

¹*Institute of Electrical Engineering, Slovak Academy of Sciences,
Dubravská 9, 84104 Bratislava, Slovakia*

²*Institute for Technical Physics, Karlsruhe Institute of Technology, 76131 Karlsruhe, Germany*

³*Applied Superconductivity and Cryoscience Group,
Department of Materials Science and Metallurgy,
University of Cambridge, 27 Charles Babbage Road,
Cambridge, CB3 0FS, United Kingdom and*

⁴*European Organization for Nuclear Research (CERN), 1211 Geneva 23, Switzerland*

(Dated: September 27, 2019)

Stacks of superconducting tapes can trap much higher magnetic fields than conventional magnets. This makes them very promising for motors and generators. However, ripple magnetic fields in these machines present a cross-field component that demagnetizes the stacks. At present, there is no quantitative agreement between measurements and modeling, mainly due to the need of a 3D model that takes the real micron-thick superconducting layer into account. This article presents 3D modeling and measurements of cross-field demagnetization in stacks of up to 5 tapes and initial magnetization modeling of stacks of up to 15 tapes. 3D modeling of the cross-field demagnetization shows that the critical current density, J_c , in the c -axis does not play a role in cross-field demagnetization. When taking the measured anisotropic magnetic field dependence of J_c into account, calculations agree with measurements with less than 4 % deviation. Then, our 3D numerical methods can realistically predict cross-field demagnetization. Due to the force-free configuration of part of the current density, J , in the stack, better agreement with experiments will require measurement of the J_c anisotropy for the whole solid angle range, including J parallel to the magnetic field.

^a Corresponding author (enric.pardo@savba.sk).

I. INTRODUCTION

Stacks of superconducting tapes after magnetization behave like permanent magnets, and hence stacks can be used as an alternative in power and magnet applications. The advantage of the stack is high trapped magnetic field. The world record of the magnetic field is 17.7 T [45] compared to around 1.3 T remnant magnetic field of conventional permanent magnets. Although superconducting bulks can also trap high magnetic fields (17.6 T [46]), stacks present additional advantages. Their Hastelloy substrate enhances mechanical properties and, the stack length is virtually unlimited with very uniform J_c , and the stack width could be as wide as 46 mm [47]. The larger continuous superconducting object results in larger trapped flux for the same maximum trapped field. A bulk mosaic made of hexagonal or square tiles traps an average flux density of around 1/3 of its maximum, while the average flux density on a stack is around 1/2 of its maximum. Then, a long stack traps 50 % more flux than an array of bulks of the same width as the stack for each bulk. The stack enables to interlay sheets of other materials to enhance physical properties, such as metal layers enhance thermal properties, soft ferromagnetic layers enhance trapped field and reduce cross-field demagnetization, at least for stacks as stand-alone objects [48].

The high trapped field and low weight is very promising for enabling fully superconducting motors and generators [49] especially for electric aircrafts [50–54], high power generators and flywheels [55] and sea transport [56, 57]. However, stacks experience transverse magnetic fields in the rotating machines, which cause demagnetization of trapped field.

There is a big effort to fully understand the cross-field demagnetization, in order to reduce demagnetization effect and extend the time of the trapped field inside the stack, as follows.

Recent measurements of stacks showed the behaviour under cross and rotating magnetic fields [48, 58]. However, theoretical study by cross-sectional approximation (2D approach) showed qualitative agreement only. The cross-field measurements on the stack with shielding tapes are shown in [59]. The 2D modelling study and measurements were presented by Campbell [60], where A -formulation is compared with Brandt and Mikitik theory [61]. Direct comparison between the 2D model and measurements were presented by Liang [62] with qualitative agreement. The reason of the poor quantitative agreement is expected to be the real 3D shape of the experimental samples, since the models assume infinitely long geometry (2D approach). In addition, there could be numerical error issues due to the low number

of elements in the thickness (only 3). The 2D model was shown by Srpcic et al [63]. The 2D and 3D models were presented only for cylindrical bulks by Fagnard et al [64] or cubic bulks by Kapolka et al [65]. However, in the overall the full 3D model of the stack of tapes is missing, where good qualitative agreement with experiments is expected.

The main reason of missing 3D models is due to the low superconducting thickness of around $1 \mu\text{m}$, and hence high aspect ratio of the elements in the mesh. Since the variation of current density across the thickness is essential for cross-field demagnetization, methods assuming the thin-film approach cannot be applied. The inaccuracy of the elongated elements leads to numerical issues such as high number of elements, instability and the non-convergence of the modelling tools. Therefore, the models often do not take the real thickness of the superconducting layer into account.

Our goal is to model Stacks with the real thickness of the superconducting layer $1.5 \mu\text{m}$ and compare the results to the measurements, being the first 3D model of the cross-field demagnetization of stacks of tapes. For this case, our method (MEMEP 3D) is more efficient than (FEM) in \mathbf{H} formulation, because, due to the thin film shape, FEM uses many elements in the air around the sample and even between thin films [66]. This situation also seems not suitable for Fast Fourier Transformation (FFT). The bulk FFT approach [67] requires a cumbersome number of elements due to the need of uniform mesh and the low film thickness. The stack approach of FFT assumes thin films for the tapes [68], which cannot describe cross-field demagnetization.

In this article we focus on the cross-field demagnetization of the stacks of tapes up to 5 tapes, the validation of our (MEMEP 3D) method by comparison of two-tapes demagnetization with FEM, the trapped field in the stack up to 15 tapes and qualitative behaviour of bulk and stack with similar parameters.

II. METHODOLOGY OF MEASUREMENTS

The study is focused on the cross-field demagnetization of a stack of tapes. The sample is prepared from 12 mm wide SuperOx tapes with stated minimum I_c of 430 A at 77 K. The thickness of the tape is around $65 \mu\text{m}$ with $1.5 \mu\text{m}$ thin superconducting (SC) layer. The tape is with $\sim 2 \mu\text{m}$ silver stabilization on each side and around $60 \mu\text{m}$ Hastelloy. The stack of tapes is formed by 5 SuperOx tapes with 3 Kapton layers between each superconducting

layer. The superconducting tape together with 3 Kapton insulators is 220 μm thick. The sensitive part of the Hall probe sensor is 1.5 mm above the top SC layer.

Cross-field demagnetization consists on the following three main steps: magnetization by field cool (FC) method, relaxation time and cross-field demagnetization. The detailed process is the following:

- The sample is placed into the electromagnet at room temperature.
- The electromagnet is ramped up to 1 T.
- The sample is cooled down in liquid nitrogen bath at 77 K.
- The electromagnet is ramped down with ramp rate 10 mT/s.
- The sample is moved into the air-core solenoid.
- The sample is left for 300 s relaxation.
- A Hall probe above the sample measured the trapped magnetic field B_t at the center.
- The solenoid magnet applied a sinusoidal transverse-(or cross) magnetic field of several amplitudes (50, 100, 150 mT) and frequencies (1, 10 Hz). The Hall probe measured the trapped field during the demagnetization.

A. Measurement set-up

The measurement set-up contains a G10-cryostat for sample holder, an iron-core Walker Scientific HV-4H electromagnet and the separated air core solenoid.

The control system [59] contains a signal generator Agilent 33220A amplified by two power supplies KEPCO BOP 2020 connected in parallel. The current in the circuit is measured by a LEM Ultrastab IT 405-S current transducer. The magnetic field is measured by an Arepoc Hall sensor LHP-MPc [69]. The circuit is monitored by custom made lab-View program.

III. MODELLING METHOD

In this article, we use two different numerical methods. Most of the calculations are made with the Minimum Electro-Magnetic Entropy Production method in 3D (MEMEP 3D), al-

though we first benchmarked this method with Finite Element Method (FEM) calculation in the \mathbf{H} formulation for simple cases in order to cross-check the numerical methods. Although, in the previous work we made a validation of the three methods by magnetization of the bulk and stacks with the tilted fields [70].

A. MEMEP 3D model

We perform most of the calculations here by MEMEP 3D [71] based on a variational principle. The mathematical formulation uses the \mathbf{T} vector defined as an effective magnetization. The effective magnetization is non-zero only inside the modelling sample, and hence the method does not solve the air domain. The incorporated isotropic power-law enables to take n values up to $n=1000$ into account. We use $n=200$ as an approximation to the Critical State Model and $n=30$ as a realistic value for the measurements. The modelling software [72] was developed in C++ and it is enhanced by parallel computation on a computer cluster [73]. The method uses hexahedric elements with high aspect ratio, up to 5000. Therefore, MEMEP can use the same modelling geometry as the measured samples. The model assumed either isotropic constant J_c , $J_c(B)$ or $J_c(B, \theta)$ from measurements, depending on the configuration, being B the magnitude of the magnetic field (we use the term “magnetic field” for both \mathbf{B} and \mathbf{H} , since for our case $\mathbf{B} = \mu_0 \mathbf{H}$) and θ is the angle between \mathbf{B} and the normal of the tape surface (figure 15 (b)).

B. FEM 3D model

The FEM model is based on the H -formulation of Maxwell’s equations implemented in the finite-element program Comsol Multiphysics [74]. Due to the necessity of simulating the air between and around the superconducting tapes typical of the FEM approach, care had to be taken in building the domains and the mesh. In order to avoid an excessive number of degrees of freedom, an approach based on sweeping a 2D geometry and mesh was followed (see Fig. 1 of [66] for an example). The external magnetic field was applied on the boundary of the air domains by means of Dirichlet boundary conditions. A magnetic field of $B_z=300$ mT was assigned to all simulated domains as initial condition.

C. Modelling conditions

The SuperOx tape contains Hastelloy, superconducting layer (SC) and the silver thin layer as it is explained in section II. However, the model takes only the superconducting layer into account. Then, the Hastelloy and silver are treated as air in the model. The “air” separation of the superconducting layers in the stack is modelled as a conducting material of high resistivity. The gap is around $200\ \mu\text{m}$, being slightly different for each studied configuration. The thickness of the SC layer depends on the goal of the study. The general qualitative study of the cross-field demagnetization uses the thickness of $10\ \mu\text{m}$ and the more precise calculation for comparison to experiments uses the real thickness of $1.5\ \mu\text{m}$.

IV. RESULTS AND DISCUSSION

There is a big effort to fully understand the cross-field demagnetization process. However, almost all studies found only qualitative agreement with measurements. We focused on 3D modelling with all finite size effects, and hence the results can be compared with measurements on short samples. For the comparison to experiments, the model assumes the real dimensions of the measured sample and measured $J_c(B, \theta)$ dependence. Before comparing to experiments, we analyse the influence of several parameters like the superconducting layer thickness and gap between tapes. For this analysis, we study first the magnetization process and later the cross-field demagnetization.

A. In-plane magnetization of single tape with thickness variation

The first study is about in-plane magnetization due to a parallel applied magnetic field. The sketch of the modelling case and the dimensions are in the figure 1. The magnetization loop is calculated only for the M_x component, because the applied magnetic field (of amplitude $50\ \text{mT}$ and $50\ \text{Hz}$ frequency) is along the x axis. We used a thicknesses of the superconducting layer d in the range from 1 to $1000\ \mu\text{m}$ for this case. We assume constant $J_c d$, being $J_c=2.72\times10^{10}\ \text{A}/\text{m}^2$ for $d=1\ \mu\text{m}$ and n -power law exponent of 30 .

The magnetization increases with tape thickness (Fig. 2 (a)). This is not the case for the Critical State Model (CSM), which we approximate as a power law with exponent $n = 200$

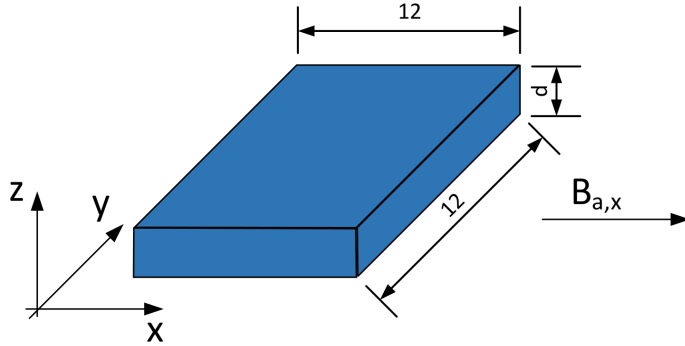


FIG. 1: Single superconducting tape for the thickness dependence study ($d=1,10,100,1000 \mu\text{m}$). Dimensions are in mm.

(Fig. 2 (a)). All magnetization loops for different thickness are within 2%, being not identical due to the power-law exponent (Fig. 2 (b)). However, commercial superconducting tapes have an n -value around 30 in self-field. The thickness dependence is due to higher electric fields from the applied magnetic field in thicker tapes. The relatively low n -value of 30 allows $J > J_c$ for high electric fields, and hence the magnetization increases with thickness roughly as 14% for each increase in thickness by a factor 10. Therefore, we already see that the sample thickness plays a role for the response to the ripple field. The effects of the thickness is much more important for the cross-field demagnetization (section IV B), which is also significant for the CSM [61, 75]. In the calculations in the following sections, we assume the real thickness of $1.5 \mu\text{m}$ for comparison to experiments and $10 \mu\text{m}$ for the purely numerical systematic analysis.

B. Cross-field demagnetization of one tape with thickness variation

A more detailed study about thickness influence is in the cross-field demagnetization. The model assumes a single tape with thickness from 1 to $100 \mu\text{m}$. The critical current density is inversely proportional to the thickness. The J_c of $1 \mu\text{m}$ tape is $J_c=2.72\times10^{10} \text{ A/m}^2$ and the n value is 30. The tape is magnetized with the perpendicular applied field to the tape surface by the Field Cool method. The field is ramped down with rate 30 mT/s over 100 s with following relaxation of 900 s . Afterwards, a sinusoidal transverse field of 500 Hz is applied along the x axis.

The demagnetization rate significantly increases with the thickness (figure 3), even though

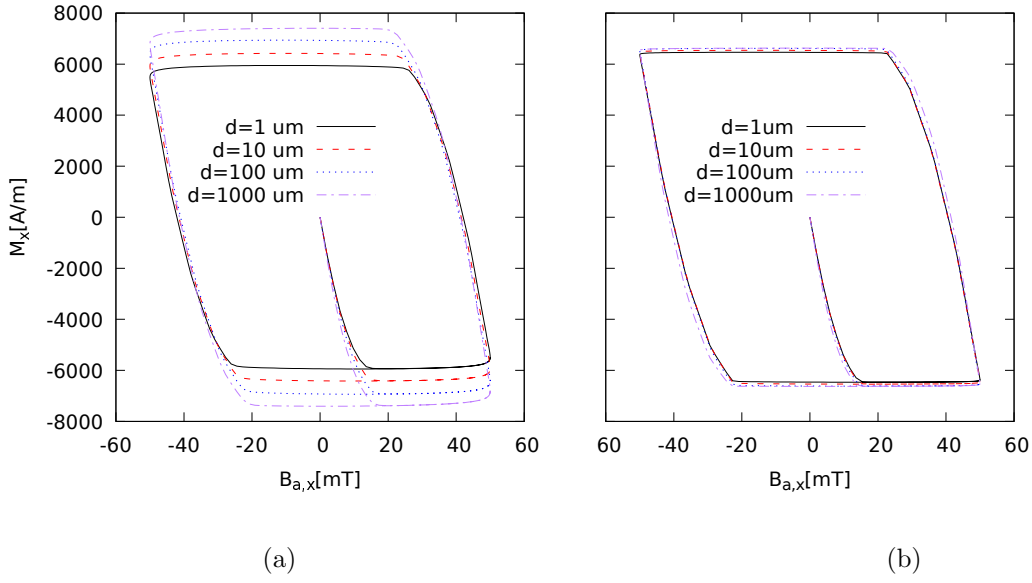


FIG. 2: Magnetization loops M_x of the single tape increases with thickness $d=(1,10,100,1000 \mu\text{m})$, while keeping the sheet critical current density $J_c d$ constant. The model assumes a realistic n power law exponent (a) $n=30$ and a situation close to the Critical State Model (b) $n=200$.

J_c is proportional to the thickness. The clear thickness dependence showed the importance of the sample thickness, as it is explained in section IV A. Therefore, the thickness in the model is very important for the cross-field demagnetization, where ripples are in the in-plane direction. The model cannot assume thicker films and lower proportionally the critical current density, as already predicted by Campbell et al [60]. Since the superconducting layer in most REBCO tapes is of the order of $1 \mu\text{m}$, 3D modelling is very challenging due to the high aspect ratio. Most previous works, which are in 2D, assumed unrealistically thicker samples due to numerical issues.

C. Trapped magnetic field in the stack of tapes

The next study is about the influence of number of tapes and gap between superconducting layers in the stack on the initial trapped field. We used the same geometrical parameters as in the previous section IV A. The superconducting layer is $10 \mu\text{m}$ thick with $J_c = 2.72 \times 10^9 \text{ A/m}^2$ and $n=30$. As shown above, it is not possible to take a larger superconductor thickness

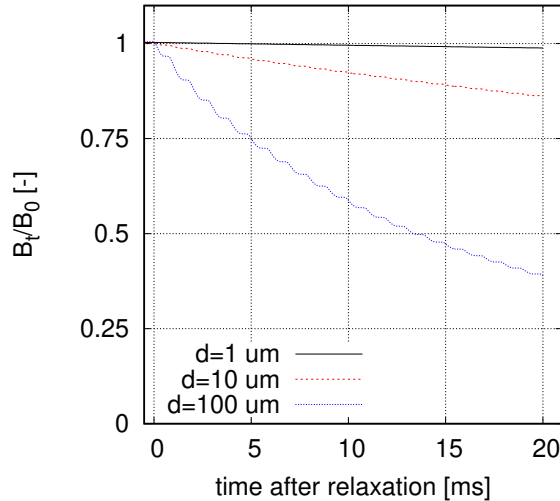


FIG. 3: The trapped field 1 mm above the single tape with thickness d in range 1-100 μm .
The 3D model assumed $n=30$.

and a proportionally lower J_c for cross-field demagnetization and transverse applied field. However, this simplification could be made for applied fields perpendicular to the tapes [76, 77]. The cause is that the electric field due to the applied magnetic field is roughly uniform in the tape thickness and the effect of the self-magnetic field can be averaged over the tape thickness.

The stack is magnetized by Field Cool (FC) method along the z axis. The initial applied magnetic field is 1 T with ramp down rate of 10 mT/s, because of the perpendicular penetration field B_p of 1 tape is 27.2 mT. Afterwards, we leave a relaxation time of 900 s, which is long enough to reach stable state of the trapped field. The trapped field decreases logarithmically during relaxation, and hence after a short time the reduction is almost negligible. The trapped field is calculated 1 mm above the top tape, similar to a Hall probe experiment. The probe position is more relevant for commercial application than the magnetic field in the tape or between the tapes. The sketch of the modelling case is on figure 5 (a).

The trapped field increases with the number of tapes figure 4. The big gap of 200 μm between SC layers causes saturation of the trapped field. The trapped field decreases with the gap g , and hence superconducting tapes with thinner Hastelloy and thermal stabilizations are more suitable for stack of the tapes based applications. The cause of the decrease in trapped field with increasing the gap is the increase of the overall thickness-to-width ratio, since the contribution of the bottom tapes to the trapped field on the top decreases with

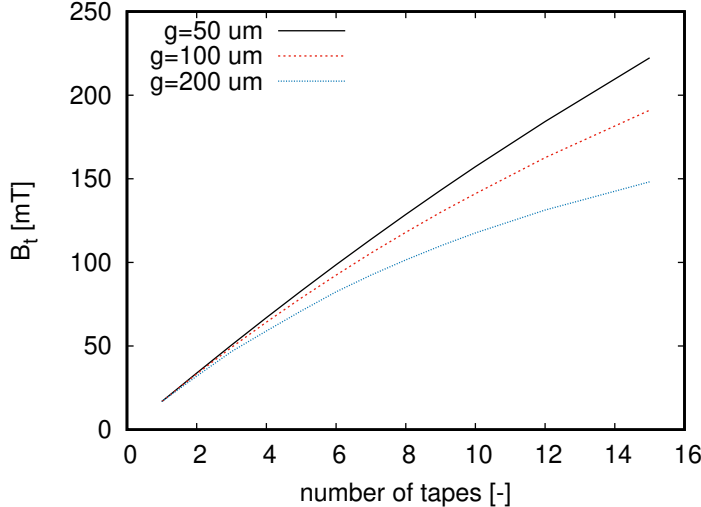


FIG. 4: The trapped field increases with the number of the tapes in the stack and reduced gap between superconducting layers. The gap is $g=50,100,200\text{ }\mu\text{m}$.

the overall thickness.

D. Benchmark of MEMEP 3D with FEM

Next, we cross-check the MEMEP 3D method and the Finite Element Method. The comparison case is for a two-tape stack only, for simplicity. The superconducting layer is $10\text{ }\mu\text{m}$ thin with $200\text{ }\mu\text{m}$ gap between the layers. The mesh contains $15 \times 15 \times 5$ cells per superconducting layer. The electrical parameters are the same as $J_c=2.72 \times 10^9\text{ A/m}^2$ and $n=30$.

The result of the trapped field 1 mm above the top surface is on figure 5 (b). The trapped field is normalized by the trapped field at the end of the relaxation time, B_0 . The value of B_0 is 32.4 mT for MEMEP 3D and 28.6 mT for FEM method. The comparison is with very good agreement, even though the trapped field is with 11% difference. The demagnetization rate is the same for both methods. The difference in the trapped field comes from the calculation of the magnetic field. The magnetization of the sample is more precise and the difference is only 4 %. Therefore, the screening current in the sample is with very good agreement. This confirms the validity of the MEMEP 3D calculations. The computing time for the case with mesh $15 \times 15 \times 5$ cells and the cross-field of 240 mT is for MEMEP 3D 3-4 hours and for FEM is 14-15 hours. The MEMEP used the computer with i7-4771 CPU at

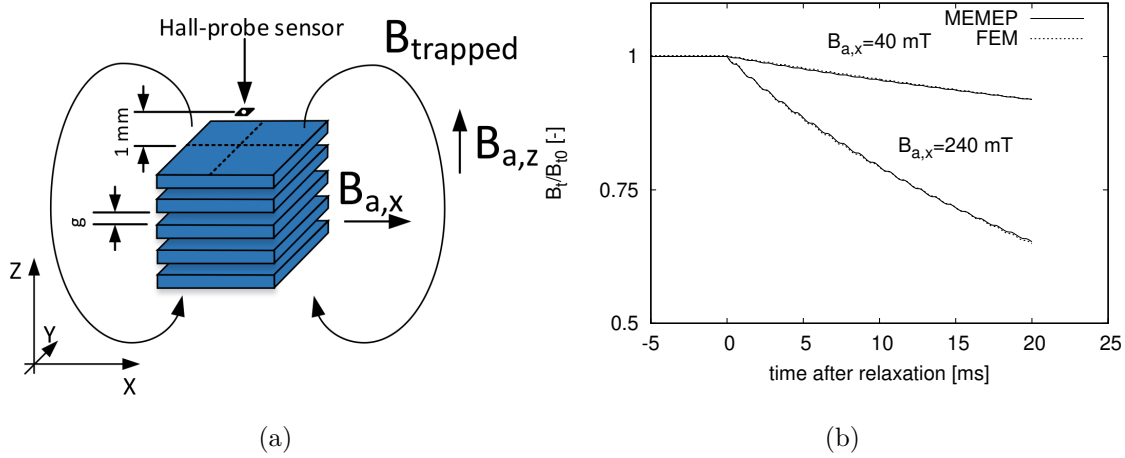


FIG. 5: (a) Stack of 5 tapes with Hall probe position and direction of the magnetization and demagnetization fields $B_{a,z}$ and $B_{a,x}$, respectively. The gap between superconducting layers is $200 \mu m$. (b) The cross-field demagnetization of a two tapes stack calculated by MEMEP 3D and FEM. The methods are in very good agreement for both cross-field amplitudes 40 mT and 240 mT.

3.5 GHz and the FEM used workstation with i7-4960X CPU at 3.60 GHz.

E. Cross-field demagnetization for high speed rotating machines (500 Hz)

The next study is about the entire cross-field demagnetization process in the stack of 5 tapes. The sketch of the modelling case is on figure 5 (a) and it uses the same parameters as in the previous sections. The gap g between superconducting layers is $200 \mu m$ and superconducting layer is $10 \mu m$ thick. The time evolution of the magnetizing field, B_{az} , and the trapped field on the stack, B_t , are on figure 8. At time 1000 s, the sinusoidal ripple field, B_{ax} , of 500 Hz is switched on.

The study of the current density inside the stack is on the x and y cross-section planes, as defined in figure 6. The current density maps (figure 7) are in the real scale except the z coordinate. Since the tapes are $10 \mu m$ thick and the gap is $200 \mu m$ wide, the variations in the thickness of the current density are not visible in the real scale. Therefore, the maps contains the real data, but superconducting cells are shown with the same high as the the gap cells. Since we use an odd number of cells in the x and y directions, there appears a

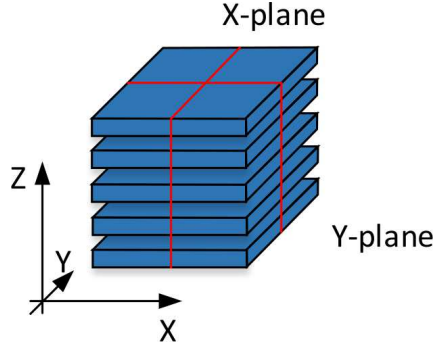


FIG. 6: The cross-sectional planes are at $x = 6$ mm and $y = 6$ mm for the current density colour maps.

central cell with zero current density in figure 7(a,d-f), causing the vertical purple line. The study case is with cross-field amplitude 240 mT.

The stack at the end of relaxation is fully saturated with $J_x \approx J_c$ and $J_y \approx J_c$ on figures 7 (a) and 7 (d), respectively. The J_z component is very small, around $0.001J_c$ due to the thin film shape. The current density magnitude is below the critical current density J_c , because of flux relaxation.

The applied cross-field at the first positive peak causes the small penetration of the screening current from top and bottom of each individual tape as seen in figure 7 (b). The penetration front on the y plane rewrites the remanent state of the current density J_y to the positive sign from the top and with negative sign from the bottom of each tape (figure 7 (b)). This process can be explained by the Bean model of the infinite thin strip [61] or other numerical 2D modelling [48, 60]. In our stack, the penetration front contains both the J_y and J_z components, even though J_z is very small. The x plane section of figures 7 (d-f) shows that the J_x current density from remanent state is progressively decreasing at each cycle by the effect of J_y (and also J_z in a lesser amount) at the penetration front at the top and bottom of each individual tape.

Finally, we study in detail the current density maps at the tenth positive peak of the cross-field. At the y plane, the J_y current density component penetrates slightly more than after the end of the 1st cycle. The penetration depth is in 2 cells from the top and bottom of each layer within the total of 9 cells per superconducting layer (figure 7 (c)). The lowest penetration is in the inner tapes. The cause is that the inductive coupling with the rest of the tapes is the largest. This enhanced inductive coupling slows down the demagnetization

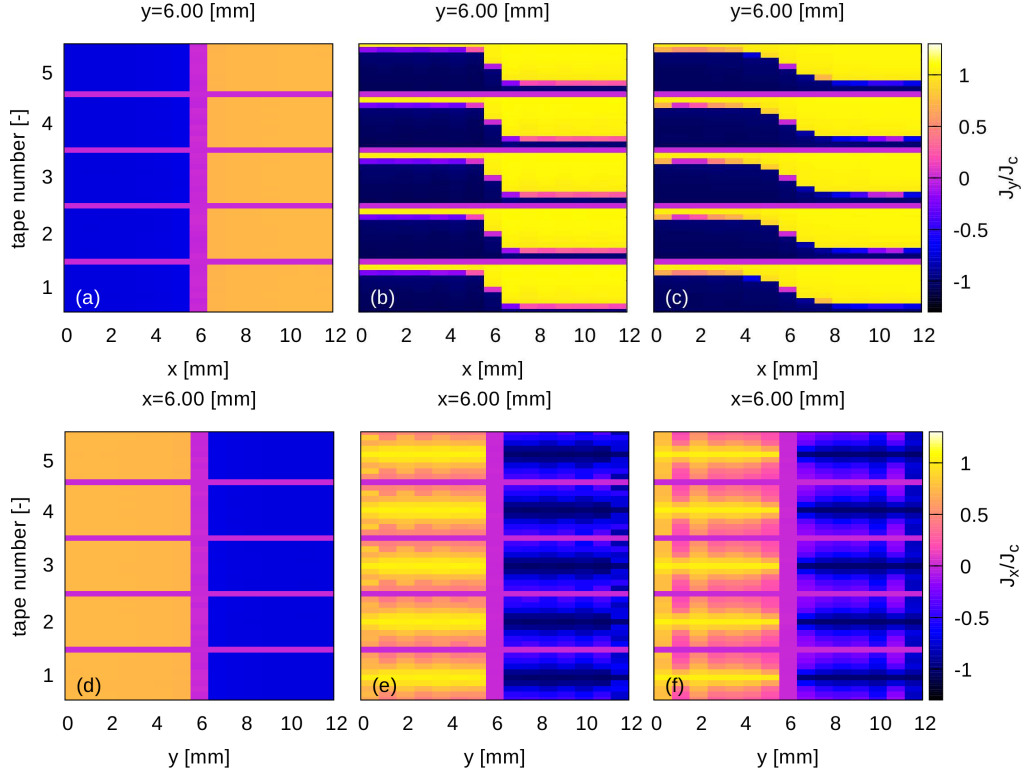


FIG. 7: 3D current density colour maps during cross-field demagnetization. The perpendicular component of the current density in the cross-sections at the middle of the stack at $x=6$ mm, $y=6$ mm, (a, d) after 15 minutes relaxation (b, e) at first positive peak of ripple field 240 mT (c,f) at last positive peak (10th cycle). The air and the superconducting cells are plotted on the colour maps with the same high for better visibility. However, the calculation uses the real dimensions of the sample.

decay due to the dynamic magneto-resistance [61, 75], being the decay exponential for large enough time. At the x -plane, the J_x component is almost completely concentrated in 3 cells in the centre of each superconducting layer (figure 7 (f)). The current maps show slow penetration of the current front and erasing process of the remnant state with increasing the number of cycles. Although J_z plays a role in the cross-field demagnetization, its value is much below J_c , and hence reducing J_c in the z direction will not cause any significant change.

The trapped magnetic field B_t during the whole process is calculated 1 mm above the top surface (figure 8). After relaxation, we applied cross-fields with two different amplitudes, 40 and 240 mT, in order to see the behaviour in the fields below and above the penetration

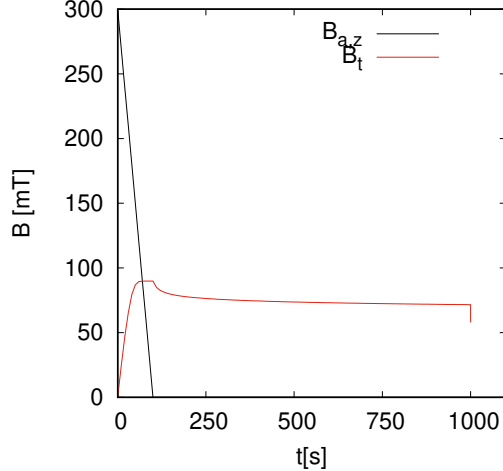


FIG. 8: Time evolution of the applied magnetic field $B_{a,z}$ and the trapped field B_t on the stack.

field B_p of the stack. The parallel penetration field $B_{p,\parallel}$ of 1 tape is 17 mT according to the slab Critical-State model [78, 79],

$$B_{p,\parallel} = \mu_0 J_c d / 2. \quad (1)$$

The demagnetization rate for 40 mT cross-field is very low, with 3.9% drop of the trapped field after 10 cycles (figure 9). The higher cross-field of 240 mT makes 19.1 % reduction of the trapped field. The roughly linear demagnetization is consistent with Brandt's predictions, where there is linear decay for the first few cycles [61]. However, the method of [61] is based on Bean model and for a single tape. For applied fields above the penetration field, as is the case of both 40 and 240 mT, demagnetization will continue until the entire sample is demagnetized.

A more detailed trapped field profile is calculated along the (red) line B_t above the sample on figure 10 (a). The profile has the usual symmetric peak at the end of the relaxation time (figure 10 (b) black curve). The first positive peak of the cross-field of 240 mT makes a small reduction of the trapped field [figure 10 (b) blue curve], since the current density has not changed significantly due to transverse field. The last positive peak of the cross-field is shown on figure 10 (b) as red line. The trapped field peak is always symmetric without any shift, contrary to cubic bulk samples [65]. The cause of this difference is the thin film shape of tapes, as follows. For the bulk, the trapped field depends on the current distribution across the thickness, with a higher contribution for J closer to the top surface. Since J does

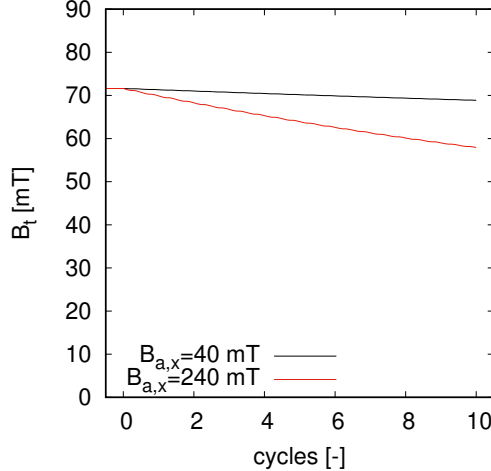


FIG. 9: The demagnetization of the trapped field by the cross-field amplitude $B_{a,x,max}$ of 40 and 240 mT and frequency 500 Hz. The demagnetization rate increases with the amplitude.

not have mirror symmetry towards the yz plane, (only inversion symmetry towards the bulk center) the trapped field on the surface is not symmetric. In contrast, the trapped field in the thin films only depends on the average J across the tape thickness, being variations on this dimension irrelevant. Since the thickness-average J does have mirror symmetry with respect to the yz plane for each tape of the stack, the trapped field on the surface also presents this mirror symmetry.

F. Comparison of cross-field demagnetization in a stack of tapes and bulk

There are two alternatives for high temperature super-magnets: stacks of tapes and bulks. Both candidates broke the world record of trapped field, being above 17 T with slightly higher values for the stack [45, 46]. However, both behave differently under cross-fields. Therefore, we performed a short simple comparison between them. We used the same geometry for 5 tapes stack as it was mentioned above. We calculated the engineering current density for the stack $J_{ce}=160$ MA/m² and set it as critical current density J_c for the bulk. The samples with the size dimensions are in figure 11. We estimated the parallel penetration field of the equivalent bulk from the slab approximation

$$B_{p,\parallel} \approx \mu_0 J_{ce} d_{all} / 2, \quad (2)$$

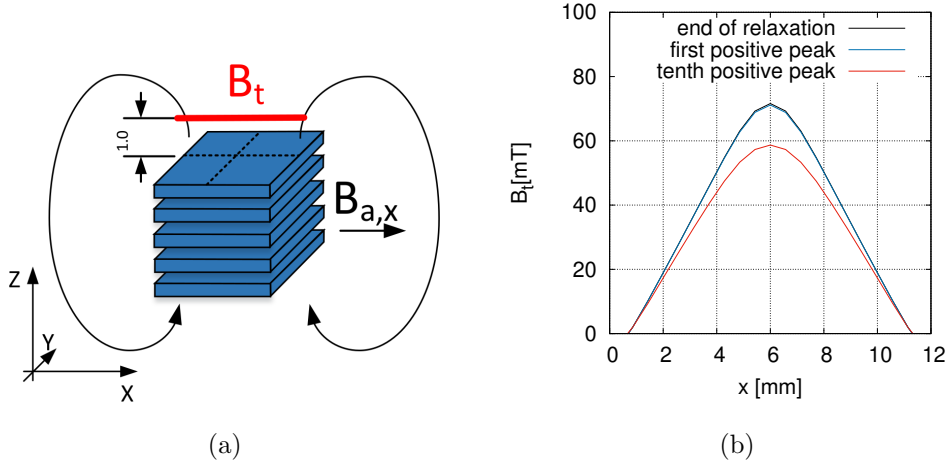


FIG. 10: (a) The position of calculated trapped field profile B_t is 1 mm above the stack. (b) The trapped field profile decreases during demagnetization by $B_{a,x}$ with amplitude 240 mT and 500 Hz.

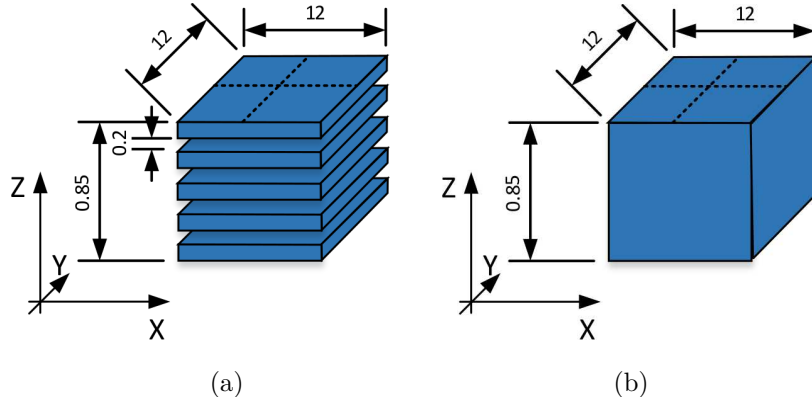


FIG. 11: Bulk and stack of tapes with the same geometrical dimensions and engineering critical current density for comparison. Dimensions are in mm.

being $d_{all}=0.85$ mm the overall stack thickness and $B_{p,\parallel,bulk} \approx 85.4$ mT.

The trapped field 1 mm above the top surface at the end of the relaxation time of 900 s is similar for the stack (71.6 mT) and the bulk (71.4 mT), because of similar parameters. The end of the relaxation time is marked as 0 cycle on figure 12. The bulk shows significant trapped field drop, around 93% in the first four cycles of 240 mT cross-field, being larger than the bulk penetration field (85 mT). In the case of low cross-field amplitude of 40 mT, the drop is around 16 %. For large number of cycles, the trapped field will decrease until

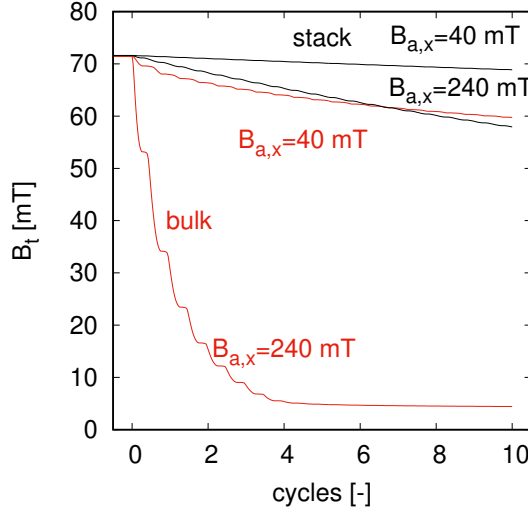


FIG. 12: The cross-field demagnetization of the bulk and stack of tapes with transverse field amplitude of 40 and 240 mT of 500 Hz.

the quasi-stable state is reached, because the ripple field amplitude is below the parallel penetration field of the bulk [61], the latter being dominated by a slow flux creep decay [63]. The stack shows much slower demagnetization rate for the high cross-field of 240 mT and the trapped field drop in 10 cycles is only 19 %. Nevertheless, demagnetization should continue until it completely demagnetizes the sample, because the ripple field is above the parallel penetration field of one tape (17 mT). The same behaviour is observed for the low cross-field of 40 mT with very low trapped field reduction of 3.9% at 10 cycles. Therefore, for the high cross-field cases (ripple field above the parallel penetration field of the bulk) the stack of tapes is more suitable. However, in the case of low fields the bulk is more suitable because the asymptotic trapped field does not vanish after many cycles. Nevertheless, if the super-magnet is submitted to relatively low number of cycles, the stack of tapes are preferred in any case. Applications with low frequency ripples and built-in re-magnetization, such as certain low-speed motors and wind turbines, might also favour stacks of tapes, because of less re-magnetization.

G. Cross-field demagnetization: measurements and modelling

The last study is about measurements and comparison with calculations. The stack consists of 5 tapes and the parameters are in the table I. The details about the sample

TABLE I: Input parameters of the measurements and calculation.

Size [mm]	12x12x0.0015
$J_{c,self}$ [A/m ²]	2.38×10^{10}
$B_{az,max}$ [T]	1.0
Ramp rate [mT/s]	10
Relaxation [s]	300
E_c [V/m]	1e-4
f_{ax} [Hz]	0.1,1
B_{ax} [mT]	50,100,150
n [-]	30

and the measurements are given in section II. The measurements are performed for two cross-field frequencies: 1 and 10 Hz.

The demagnetization rate increases with the field (figure 13 (a)). The higher demagnetization rate for 10 Hz is due to 10 times more cycles per second, and hence the demagnetization rate per cycle at low frequencies depends on the frequency only slightly [59]. However, the measurements showed increased frequency dependence with field (figure 13 (b)). The reason is that the higher frequency of the applied field causes higher electric field, and hence the current density increases. This reduces both the penetration field and the demagnetization rate [65, 77, 80–82]. The calculation uses the same parameters as the measurements (table I).

The model uses 1.5 μ m thin superconducting layer with 220 μ m gap between them. The first comparison is with constant J_c (figure 14). The minimum stated I_c of the SuperOx tape is 430 A at self-field (or $J_c=2.38 \times 10^{10}$ A/m²). We reduced J_c by 22% to the value $J_c=1.85 \times 10^{10}$ A/m², in order to get similar trapped field, 58.9 mT, at the end of the relaxation time as the measurements, 58.1 mT. The demagnetization rate is lower than the measured one. The reason is that the assumed critical current density is too high, because of the missing $J_c(B, \theta)$ dependence in the model. The magnetic field reduces the critical current

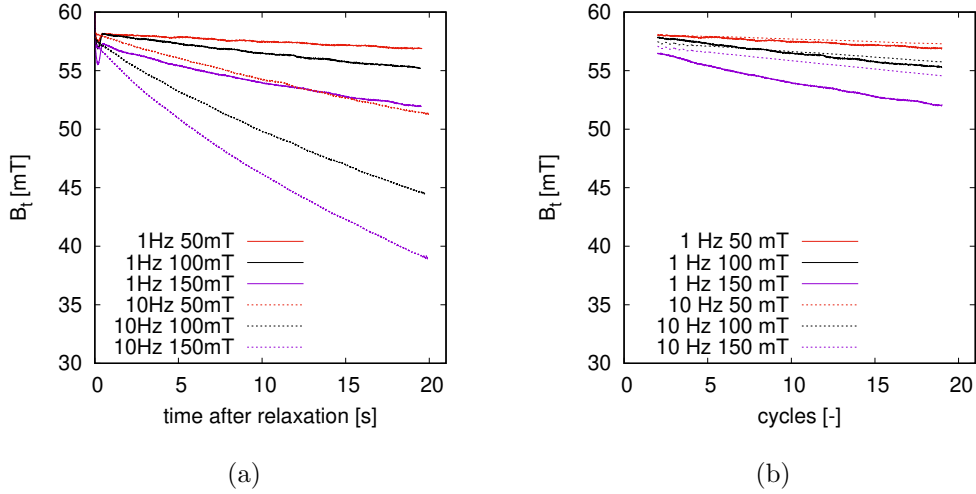


FIG. 13: (a) The cross-field demagnetization measurements with cross-field frequency of 1 and 10 Hz. The demagnetization rate increases with the cross-field amplitude. (b) The cross-field demagnetization as the function of number of cycles. There is low frequency dependence. However, the demagnetization rate is similar for both frequencies.

density, and hence it increases the demagnetization rate.

Another comparison between the model with $J_c(B)$ dependence and measurements is on the figure 16. The $J_c(B)$ data was measured on the 4 mm wide SuperOx tape (figure 15). The critical current per tape width at self-field for the measured tape (37.8 A/mm) is roughly the same as the 12 mm wide tape used in the stack (35.8 A/mm), being the latter value the minimum stated one by the producer. The theoretical difference is 5%, which is very small. The average tape I_c could be higher, around 440 A or 450 A regarding typical deviations in SuperOx tapes, and hence even more close to that in the calculations. By now, we assume an isotropic $J_c(B)$ dependence, taking the measured $J_c(B, \theta)$ values at perpendicular applied field. Then, we assume an isotropic angular dependence in the model. The cross-field is parallel to the tape surface, and hence the actual critical current density is larger than that in the model, also presenting lower reduction under magnetic fields than assumed. This is the reason why the demagnetization rate is overestimated for the high cross-fields of 100 mT and 150 mT.

The last comparison here uses the measured $J_c(B, \theta)$ dependence. Now, the model agrees very well with measurements (figure 17). The lowest deviation at the last cycle is 0.2 % is for 50 mT and 1.2 % for 100 mT cross-field. The higher cross-field shows higher demagnetization

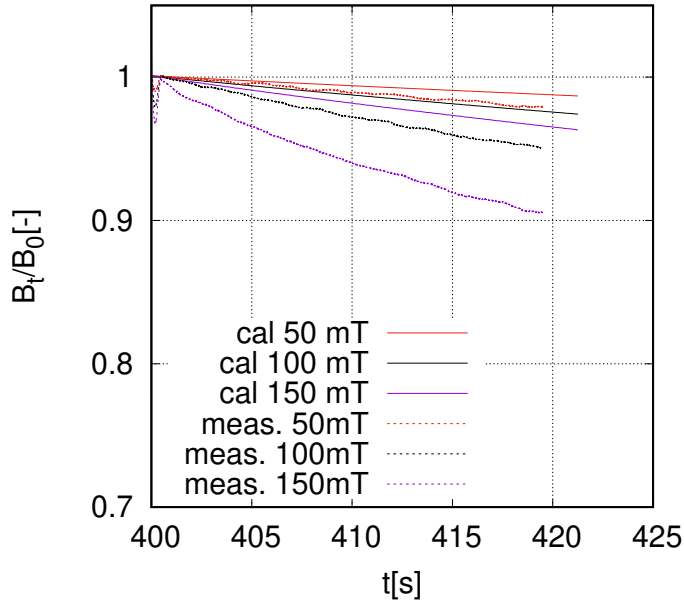


FIG. 14: Comparison of the measurements and calculations (constant $J_c = 1.85 \times 10^{10}$ A/m²) of 1 Hz cross-field demagnetization. The constant J_c underestimates the demagnetization rate due to missing $J_c(B)$ dependence.

rate in the calculation, being the difference is 4.0 %. We also study the effect of the measured $n(B, \theta)$ dependence (figure 18 (a)) compared to the constant $n = 30$ assumption. The demagnetization rate is slightly changed with $n(B, \theta)$ dependence (figure 18 (b)). The local J increases with decreasing the n value, and hence it changes the demagnetization rate. There is a slight reduction of the demagnetization rate at the first few cross-field cycles. However, later on the demagnetization rate overlaps with the constant n curve and slightly increased. The demagnetization rate is more influenced for cross-field above 50 mT.

There are several reasons for reduction of the accuracy in the model. The $J_c(B, \theta)$ data covers correctly only the J_c in the y -plane position (figure 6), where the current is perpendicular to the magnetic field. However, at the x -plane, the current density presents a large component parallel to the applied magnetic field, being in the x direction. This is the so-called force-free configuration [83], where J_c should be different than the typical $J_c(B, \theta)$ measurements with \mathbf{B} always perpendicular to the transport direction. Since J_c in force-free configuration is often higher [84], this could explain the overestimated cross-field demagnetization in the model. Measurements of bulk angular dependence, $J_c(B, \theta, \phi)$ with ϕ being the angle of \mathbf{B} with the current density, are scarce for any type of sample [84] and

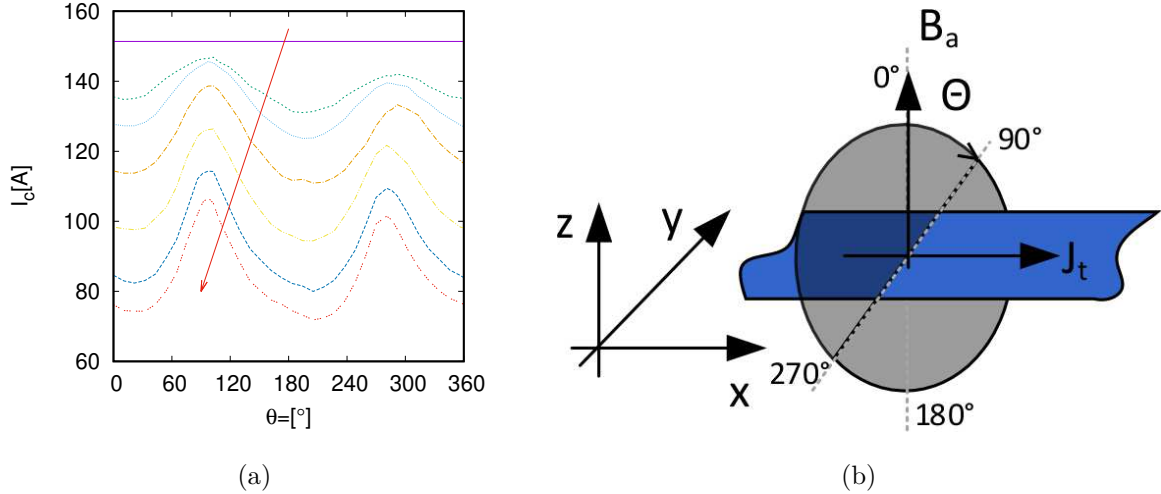


FIG. 15: (a) The $I_c(B, \theta)$ measured data on a 4 mm wide SuperOx tape with the applied field amplitude ($B_{a,max}=0, 36, 49, 72, 100, 144, 180$ mT). (b) The sketch of the $I_c(B, \theta)$ measurements with the definition of the θ angle to the tape surface.

missing for this particular tape. The cause is the complexity of the measurements, requiring a double goniometer [85–88]. The model uses $J_c(B, \theta)$ data for both components J_x and J_y , and hence there is discrepancy between the model and the real measurements in the highest cross-fields.

V. CONCLUSIONS

The current article analysed both the measurements and 3D modelling of the cross-field demagnetization of a stack of up to 5 REBCO tapes. The MEMEP 3D modelling tool showed the full cross-field demagnetization process in the 5 tapes stack with 3D screening current path. The screening current from the cross-field penetrates into the sample and reduces the trapped field.

The comparison of the MEMEP 3D calculation results with FEM for a two-tape stack showed very good agreement, cross-validating the methods. The calculation showed that in the in-plane magnetization case, the magnetization changes by 14 % for each increase of the superconducting layer thickness by factor 10, and hence the models cannot assume thicker layers with the proportional critical current density in the transverse field. For cross-field demagnetization, the thickness dependence is even more pronounced, being also important

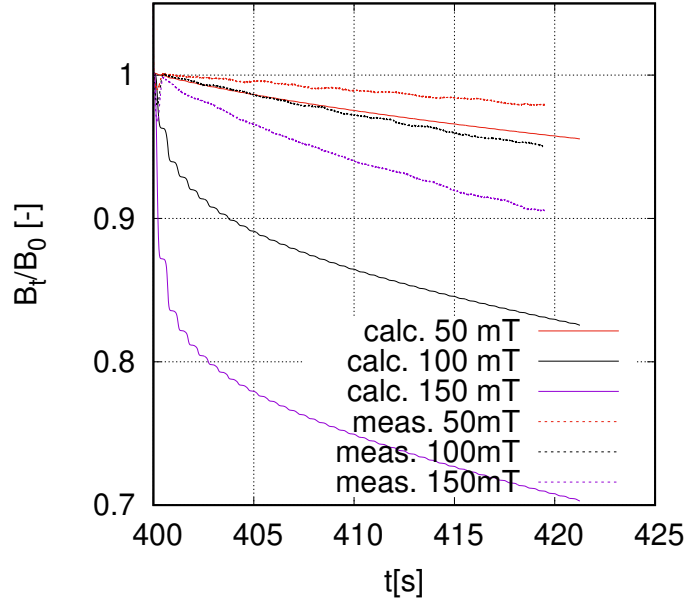


FIG. 16: Comparison of the measurements and calculations with $J_c(B)$ measured data of 1 Hz cross-field. The $J_c(B)$ dependence overestimates the demagnetization rate due to missing anisotropy dependence.

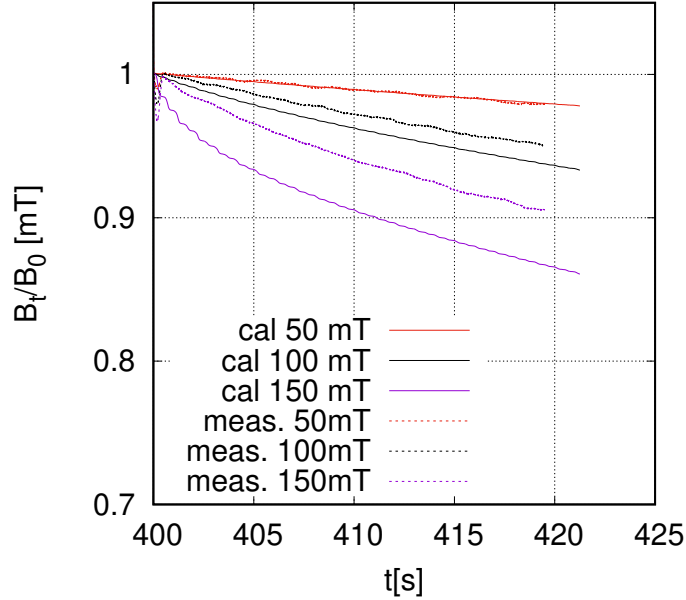


FIG. 17: The comparison of measurements and calculations with $J_c(B, \theta)$ measured data of 1 Hz transverse field. The calculation agrees very well for low cross-field up to 50 mT. The cross-field above 50 mT requires $J_c(B, \theta)$ measured data with a parallel component to the current path. However, the results for higher fields are with good accuracy, around 4%.

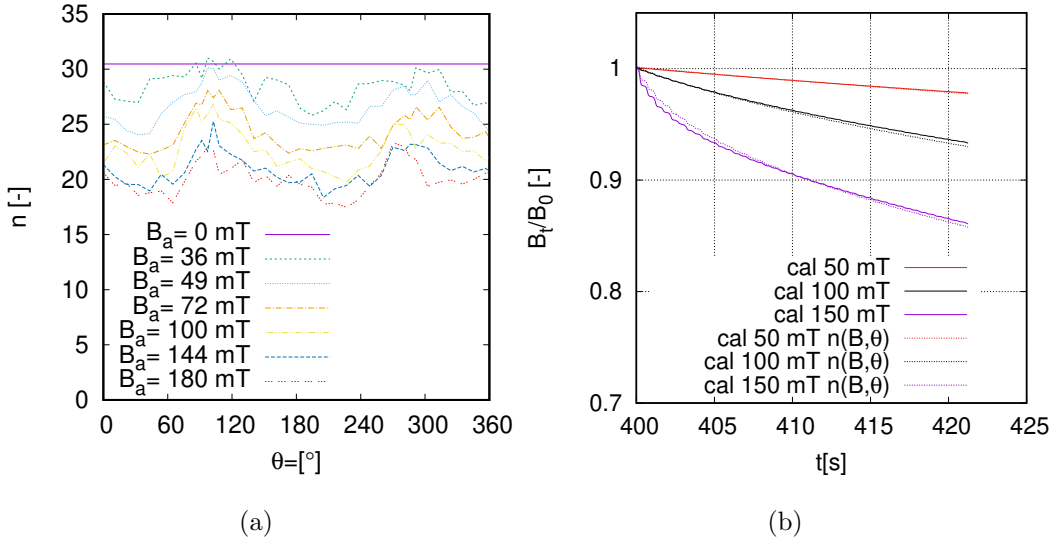


FIG. 18: (a) The $n(B, \theta)$ measured data on a 4 mm wide SuperOx tape. (b) The comparison of calculation with constant $n=30$ and $n(B, \theta)$ dependence, both cases use $J_c(B, \theta)$ dependence. Using $n(B, \theta)$ slightly reduces the demagnetization rate for a few number of cycles, but later on it is increased slightly.

for the CSM. Since the REBCO tapes are usually as thin as few microns, the model has to assume the same thickness, in order to reach quantitative agreement. The trapped field in the stack of tapes decreases with the thickness of the substrate or spacer, and therefore thinner substrates and stabilizations are more suitable. We also compared the stack with the equivalent bulk. The stack demagnetizes slower. However, we expect that the bulk reaches an stable state without further drop of the trapped field under cross-fields lower than the penetration field.

The measurements of the 5 tapes stack assembled from 12 mm wide SuperOx tapes showed increased demagnetization rate with the cross-field. The comparison with the calculations revealed that the constant J_c and isotropic $J_c(B)$ dependences are not sufficient for cross-field modelling, and $J_c(B, \theta)$ dependence is necessary. The MEMEP 3D calculations reached 4% accuracy with the measurements and pointed out the importance of the $J_c(B, \theta, \phi)$ for the high cross-field amplitudes for more accurate predictions. The $n(B, \theta)$ dependence showed a slight influence on the demagnetization rate.

In conclusion, we have shown that 3D modelling can qualitatively predict cross-field demagnetization in stacks of tapes, contrary to previous 2D modelling. This qualitative study

has been possible thanks to the computing efficiency and parallelization of the MEMEP 3D method. The analysis here suggests that force-free effects may be important in the measured samples, pointing out the need of $J_c(B, \theta, \phi)$ measurements over the whole solid angle range.

ACKNOWLEDGEMENTS

We acknowledge M vojenčiak for the critical current and power-law exponent measurements and A Patel for discussions. The authors acknowledge the financial support by the European Union's Horizon 2020 research innovation program under grant agreement No 7231119 (ASuMED consortium). M.K. and E.P. acknowledge the use of computing resources provided by the project SIVVP, ITMS 26230120002 supported by the Research & Development Operational Programme funded by the ERDF, the financial support of the Grant Agency of the Ministry of Education of the Slovak Republic and the Slovak Academy of Sciences (VEGA) under contract No. 2/0097/18, and the support by the Slovak Research and Development Agency under the contract No. APVV-14-0438.

[1] A. Patel, A. Baskys, T. Mitchell-Williams, A. McCaul, W. Coniglio, J. Hanisch, M. Lao, and B. A. Glowacki. A trapped field of 17.7 T in a stack of high temperature superconducting tape. *Supercond. Sci. Technol.*, 31(9):09LT01, 2018. DOI: 10.1088/1361-6668/aad34c.

[2] J. H. Durrell, A. R. Dennis, J. Jaroszynski, M. D. Ainslie, K. G. B. Palmer, Y. H. Shi, A. C. Campbell, J. Hull, M. Strasik, E. E. Hellstrom, and D. A. Cardwell. A trapped field of 17.6T in melt-processed, bulk Gd-Ba-Cu-O reinforced with shrink-fit steel. *Supercond. Sci. Technol.*, 27:5, 2014.

[3] M. W. Rupich, S. Sathyamurthy, S. Fleshler, Q. Li, V. Solovyov, T. Ozaki, U. Welp, WK. Kwok, M. Leroux, and AE. Koshelev. Engineered pinning landscapes for enhanced 2G coil wires. *IEEE Trans. Appl. Supercond.*, 26(6601904), 2016. DOI: 10.1109/TASC.2016.2542270.

[4] M. Baghdadi, H. S. Ruiz, and T. A. Coombs. Nature of the low magnetization decay on stacks of second generation superconducting tapes under crossed and rotating magnetic field experiments. *Scientific reports.*, 8(1342), 2018.

[5] K. S. Haran, S. Kalsi, T. Arndt, H. Karmaker, R. Badcock, B. Buckley, T. Haugan, M. Izumi, D. Loder, J. W. Bray, P. Masson, and E. W. Stautner. High power density superconducting rotating machines development status and technology roadmap. *Supercond. Sci. Technol.*, 30:123002, 2017. <https://doi.org/10.1088/1361-6668/aa833e>.

[6] Horizon 2020, ASuMED <https://ec.europa.eu/inea/en/horizon-2020/projects/h2020-transport/aviation/asumed>.

[7] E. Pardo, F. Grilli, Y. Liu, S. Wolftadler, and T. Reis. AC loss modeling in superconducting coils and motors with parallel tapes as conductor. *IEEE Trans. Appl. Supercond.*, 29(5):5pp, 2019.

[8] A. Patel, V. Climente-Alarcon, A. Baskys, B. Glowacki, and T. Reis. Design considerations for fully superconducting synchronous motors aimed at future electric aircraft. *2018 IEEE INTERNATIONAL CONFERENCE ON ELECTRICAL SYSTEMS FOR AIRCRAFT...*, (ISBN:978-1-5386-4192-7), 2018.

[9] P. J. Masson, K. Ratelle, P. A. Delobel, A. Lipardi, and C. Lorin. Development of a 3D sizing model for all-superconducting machines for turbo-electric aircraft propulsion. *IEEE Trans. Appl. Supercond.*, 23(3):3600805, 2013.

[10] F. Berg, J. Palmer, P. Miller, and G. Dodds. HTS system and component targets for a distributed aircraft propulsion system. *IEEE Trans. Appl. Supercond.*, 27:4, 2017.

[11] K. Matsunaga, M. Tomita, N. Yamachi, K. Iida, J. Yoshioka, and M. Murakami. Ybco bulk of the superconducting bearing for a 10 kwh flywheel. *Supercond. Sci. Technol.*, 15(5):842–845, 2002.

[12] T. Yanamoto, M. Izumi, K. Umemoto, T. Oryu, Y. Murase, and M. Kawamura. Load test of 3-MW HTS motor for ship propulsion. *IEEE Trans. Appl. Supercond.*, 27(5204305), 2017.

[13] B. Gamble, G. Snitchler, and T. MacDonald. Full power test of a 36.5 MW HTS propulsion motor. *IEEE Trans. Appl. Supercond.*, 21(3):1083–1088, 2011.

[14] M. Baghdadi, H. S. Ruiz, and T. A. Coombs. Crossed-magnetic-field experiments on stacked second generation superconducting tapes: Reduction of the demagnetization effects. *Appl. Phys. Lett.*, 104(232602), 2014.

[15] A. Baskys, A. Patel, and B. A. Glowacki. Measurements of crossed-field demagnetisation rate of trapped field magnets at high frequencies and below 77k. *Supercond. Sci. Technol.*, 31:065011, 2018.

- [16] A. Campbell, M. Baghdadi, A. Patel, D. Zhou, K. Y. Huang, Y. Shi, and T. Coombs. Demagnetisation by crossed fields in superconductors. *Supercond. Sci. Technol.*, 30, 2017.
- [17] E.H. Brandt and G.P. Mikitik. Why an ac magnetic field shifts the irreversibility line in type-II superconductors. *Phys. Rev. Lett.*, 89(2):27002, 2002.
- [18] F. Liang, T. Qu, Z. Zhang, J. Sheng, W. Yuan., Y. Iwasa, and M. Zhang. Vortex shaking study of rebco tape with consideration of anisotropic characteristics. *Supercond. Sci. Technol.*, 30:094006, 2017.
- [19] J. Srpcic, F. Perez, K. Y. Huang, Y. Shi, M. D. Ainslie, A. R. Dennis, M. Filipenko, M. Boll, D. A. Cardwell, and J. H. Durrell. Penetration depth of shielding currents due to crossed magnetic fields in bulk (RE)-Ba-Cu-O superconductors. 32:035010, 2019.
- [20] J. F. Fagnard, M. Morita, S. Nariki, H. Teshima, H. Caps, B. Vanderheyden, and P. Vandebemden. Magnetic moment and local magnetic induction of superconducting/ferromagnetic structures subjected to crossed fields: experiments on gdbco and modeling. *Supercond. Sci. Technol.*, 29, 2016.
- [21] M. Kapolka, J. Srpcic, D. Zhou, M. Ainslie, E. Pardo, and A. Dennis. Demagnetization of cubic Gd-Ba-Cu-O bulk superconductor by cross-fields: measurements and 3D modelling. *IEEE Trans. Appl. Supercond.*, 28:6801405, 2018. DOI: 10.1109/TASC.2018.2808401.
- [22] F. Grilli, R. Brambilla, F. Sirois, A. Stenvall, and S. Memiaghe. Development of a three-dimensional finite-element model for high-temperature superconductors based on the H -formulation. *Cryogenics*, 53:142–147, 2013.
- [23] L. Prigozhin and V. Sokolovsky. Fast fourier transform-based solution of 2D and 3D magnetization problems in type-II superconductivity. *Supercond. Sci. Technol.*, 31:055018, 2018. DOI: 10.1088/1361-6668/aab75d.
- [24] L. Prigozhin and V. Sokolovsky. Solution of 3D magnetization problems for superconducting film stacks. *Supercond. Sci. Technol.*, 31:125001, 2018. DOI: 10.1088/1361-6668/aadff8.
- [25] Multi-7U,available online at: <http://www.arepoc.sk/?p=29>.
- [26] M. Kapolka, V. M. R. Zermenio, S. Zou, A. Morandi, P. L. Ribani, E. Pardo, and F. Grilli. Three-dimensional modeling of the magnetization of superconducting rectangular-based bulks and tape stacks. *IEEE Trans. Appl. Supercond.*, 28:8201206, 2018. DOI: 10.1109/TASC.2018.2801322.

- [27] E. Pardo and M. Kapolka. 3D computation of non-linear eddy currents: variational method and superconducting cubic bulk. *J. Comput. Phys.*, 344:339–363, 2017.
- [28] E. Pardo and M. Kapolka. 3D magnetization currents, magnetization loop, and saturation field in superconducting rectangular prisms. *Supercond. Sci. Technol.*, 30:064007, 2017.
- [29] Computer cluster, available online at: <http://hpc.ui.savba.sk/index.php?page=klaster>.
- [30] R. Brambilla, F. Grilli, and L. Martini. Development of an edge-element model for AC loss computation of high-temperature superconductors. *Supercond. Sci. Technol.*, 20(1):16–24, 2007.
- [31] E. H. Brandt and G. P. Mikitik. Vortex shaking and magnetic relaxation in superconductors. *Physica C*, 408-410:514–515, 2004.
- [32] E. Pardo and F. Grilli. Numerical simulations of the angular dependence of magnetization ac losses: coated conductors, roebel cables and double pancake coils. *Supercond. Sci. Technol.*, 25:014008, 2012.
- [33] F. Grilli, E. Pardo, A. Stenvall, D. N. Nguyen, W. Yuan, and F. Gömöry. Computation of losses in HTS under the action of varying magnetic fields and currents. *IEEE Trans. Appl. Supercond.*, 24(1):8200433, 2014.
- [34] C.P. Bean. Magnetization of high-field superconductors. *Rev. Mod. Phys.*, 36(1):31–38, 1964.
- [35] C. Navau, N. Del-Valle, and A. Sanchez. Macroscopic modeling of magnetization and levitation of hard type-II superconductors: The critical-state model. *IEEE Trans. Appl. Supercond.*, 23(1):8201023, 2013.
- [36] M. Sander and F. Grilli. FEM-calculations on the frequency dependence of hysteretic losses in coated conductors. *J. Phys. Conference Series*, 234:022030, 2010. DOI: 10.1088/1742-6596/234/2/022030.
- [37] K. P. Thakur, A. Raj, E. H. Brandt, J. Kvitkovic, and S. V. Pamidi. Frequency-dependent critical current and transport ac loss of superconductor strip and roebel cable. *Supercond. Sci. Technol.*, 24(065024), 2011. DOI: 10.1088/0953-2048/24/6/065024.
- [38] K. P. Thakur, A. Raj, E. H. Brandt, and P. Sastry. Frequency dependent magnetization of superconductor strip. *Supercond. Sci. Technol.*, 24:045006, 2011. DOI: 10.1088/0953-2048/24/4/045006.
- [39] M. Kapolka and E. Pardo. 3D modelling of macroscopic force-free effects in superconducting thin films and rectangular prisms. *Supercond. Sci. Technol.*, 32:054001, 2019.

[40] J.R. Clem, M. Weigand, J. H. Durrell, and A. M. Campbell. Theory and experiment testing flux-line cutting physics. *Supercond. Sci. Technol.*, 24:062002, 2011.

[41] J. H. Durrell, M. J. Hogg, F. Kahlmann, Z. H. Barber, M. G. Blamire, and J. E. Evetts. Critical current of $\text{YBa}_2\text{Cu}_3\text{O}_{7-\delta}$ low-angle grain boundaries. *Phys. Rev. Lett.*, 90(24), 2003. DOI: 10.1103/PhysRevLett.90.247006.

[42] R. Herzog and J. E. Evetts. Low-temperature two-axis goniometer with accurate temperature control. *Rev. of Sci. Instruments*, 65:3574, 94.

[43] T. D. Withnell, K. R. Schoppl, J. H. Durrell, and H. W. Weber. Effects of irradiation on vicinal YBCO thin films. *IEEE Trans. Appl. Supercond.*, 19:3, 2009. DOI: 10.1109/TASC.2009.2019240.

[44] M. Lao, J. Hecher, M. Sieger, P. Pahlke, M. Bauer R. Huhne, and M. Eisterer. Planar current anisotropy and field dependence of J_c in coated conductors assessed by scanning hall probe microscopy. *Supercond. Sci. Technol.*, 30:024004, 2017.

[45] A. Patel, A. Baskys, T. Mitchell-Williams, A. McCaul, W. Coniglio, J. Hanisch, M. Lao, and B. A. Glowacki. A trapped field of 17.7 T in a stack of high temperature superconducting tape. *Supercond. Sci. Technol.*, 31(9):09LT01, 2018. DOI: 10.1088/1361-6668/aad34c.

[46] J. H. Durrell, A. R. Dennis, J. Jaroszynski, M. D. Ainslie, K. G. B. Palmer, Y. H. Shi, A. C. Campbell, J. Hull, M. Strasik, E. E. Hellstrom, and D. A. Cardwell. A trapped field of 17.6T in melt-processed, bulk Gd-Ba-Cu-O reinforced with shrink-fit steel. *Supercond. Sci. Technol.*, 27:5, 2014.

[47] M. W. Rupich, S. Sathyamurthy, S. Fleshler, Q. Li, V. Solovyov, T. Ozaki, U. Welp, WK. Kwok, M. Leroux, and AE. Koshelev. Engineered pinning landscapes for enhanced 2G coil wires. *IEEE Trans. Appl. Supercond.*, 26(6601904), 2016. DOI: 10.1109/TASC.2016.2542270.

[48] M. Baghdadi, H. S. Ruiz, and T. A. Coombs. Nature of the low magnetization decay on stacks of second generation superconducting tapes under crossed and rotating magnetic field experiments. *Scientific reports.*, 8(1342), 2018.

[49] K. S. Haran, S. Kalsi, T. Arndt, H. Karmaker, R. Badcock, B. Buckley, T. Haugan, M. Izumi, D. Loder, J. W. Bray, P. Masson, and E. W. Stautner. High power density superconducting rotating machines development status and technology roadmap. *Supercond. Sci. Technol.*, 30:123002, 2017. <https://doi.org/10.1088/1361-6668/aa833e>.

[50] Horizon 2020, ASuMED <https://ec.europa.eu/inea/en/horizon-2020/projects/h2020-transport/aviation/asumed>.

[51] E. Pardo, F. Grilli, Y. Liu, S. Wolftadler, and T. Reis. AC loss modeling in superconducting coils and motors with parallel tapes as conductor. *IEEE Trans. Appl. Supercond.*, 29(5):5pp, 2019.

[52] A. Patel, V. Climente-Alarcon, A. Baskys, B. Glowacki, and T. Reis. Design considerations for fully superconducting synchronous motors aimed at future electric aircraft. *2018 IEEE INTERNATIONAL CONFERENCE ON ELECTRICAL SYSTEMS FOR AIRCRAFT...*, (ISBN:978-1-5386-4192-7), 2018.

[53] P. J. Masson, K. Ratelle, P. A. Delobel, A. Lipardi, and C. Lorin. Development of a 3D sizing model for all-superconducting machines for turbo-electric aircraft propulsion. *IEEE Trans. Appl. Supercond.*, 23(3):3600805, 2013.

[54] F. Berg, J. Palmer, P. Miller, and G. Dodds. HTS system and component targets for a distributed aircraft propulsion system. *IEEE Trans. Appl. Supercond.*, 27:4, 2017.

[55] K. Matsunaga, M. Tomita, N. Yamachi, K. Iida, J. Yoshioka, and M. Murakami. Ybco bulk of the superconducting bearing for a 10 kwh flywheel. *Supercond. Sci. Technol.*, 15(5):842–845, 2002.

[56] T. Yanamoto, M. Izumi, K. Umemoto, T. Oryu, Y. Murase, and M. Kawamura. Load test of 3-MW HTS motor for ship propulsion. *IEEE Trans. Appl. Supercond.*, 27(5204305), 2017.

[57] B. Gamble, G. Snitchler, and T. MacDonald. Full power test of a 36.5 MW HTS propulsion motor. *IEEE Trans. Appl. Supercond.*, 21(3):1083–1088, 2011.

[58] M. Baghdadi, H. S. Ruiz, and T. A. Coombs. Crossed-magnetic-field experiments on stacked second generation superconducting tapes: Reduction of the demagnetization effects. *Appl. Phys. Lett.*, 104(232602), 2014.

[59] A. Baskys, A. Patel, and B. A. Glowacki. Measurements of crossed-field demagnetisation rate of trapped field magnets at high frequencies and below 77k. *Supercond. Sci. Technol.*, 31:065011, 2018.

[60] A. Campbell, M. Baghdadi, A. Patel, D. Zhou, K. Y. Huang, Y. Shi, and T. Coombs. Demagnetisation by crossed fields in superconductors. *Supercond. Sci. Technol.*, 30, 2017.

[61] E.H. Brandt and G.P. Mikitik. Why an ac magnetic field shifts the irreversibility line in type-II superconductors. *Phys. Rev. Lett.*, 89(2):27002, 2002.

[62] F. Liang, T. Qu, Z. Zhang, J. Sheng, W. Yuan., Y. Iwasa, and M. Zhang. Vortex shaking study of rebco tape with consideration of anisotropic characteristics. *Supercond. Sci. Technol.*, 30:094006, 2017.

[63] J. Srpcic, F. Perez, K. Y. Huang, Y. Shi, M. D. Ainslie, A. R. Dennis, M. Filipenko, M. Boll, D. A. Cardwell, and J. H. Durrell. Penetration depth of shielding currents due to crossed magnetic fields in bulk (RE)-Ba-Cu-O superconductors. 32:035010, 2019.

[64] J. F. Fagnard, M. Morita, S. Nariki, H. Teshima, H. Caps, B. Vanderheyden, and P. Vandebemden. Magnetic moment and local magnetic induction of superconducting/ferromagnetic structures subjected to crossed fields: experiments on gdbco and modeling. *Supercond. Sci. Technol.*, 29, 2016.

[65] M. Kapolka, J. Srpcic, D. Zhou, M. Ainslie, E. Pardo, and A. Dennis. Demagnetization of cubic Gd-Ba-Cu-O bulk superconductor by cross-fields: measurements and 3D modelling. *IEEE Trans. Appl. Supercond.*, 28:6801405, 2018. DOI: 10.1109/TASC.2018.2808401.

[66] F. Grilli, R. Brambilla, F. Sirois, A. Stenvall, and S. Memiaghe. Development of a three-dimensional finite-element model for high-temperature superconductors based on the H -formulation. *Cryogenics*, 53:142–147, 2013.

[67] L. Prigozhin and V. Sokolovsky. Fast fourier transform-based solution of 2D and 3D magnetization problems in type-II superconductivity. *Supercond. Sci. Technol.*, 31:055018, 2018. DOI: 10.1088/1361-6668/aab75d.

[68] L. Prigozhin and V. Sokolovsky. Solution of 3D magnetization problems for superconducting film stacks. *Supercond. Sci. Technol.*, 31:125001, 2018. DOI: 10.1088/1361-6668/aadffb.

[69] Multi-7U,available online at: <http://www.arepoc.sk/?p=29>.

[70] M. Kapolka, V. M. R. Zermen, S. Zou, A. Morandi, P. L. Ribani, E. Pardo, and F. Grilli. Three-dimensional modeling of the magnetization of superconducting rectangular-based bulks and tape stacks. *IEEE Trans. Appl. Supercond.*, 28:8201206, 2018. DOI: 10.1109/TASC.2018.2801322.

[71] E. Pardo and M. Kapolka. 3D computation of non-linear eddy currents: variational method and superconducting cubic bulk. *J. Comput. Phys.*, 344:339–363, 2017.

[72] E. Pardo and M. Kapolka. 3D magnetization currents, magnetization loop, and saturation field in superconducting rectangular prisms. *Supercond. Sci. Technol.*, 30:064007, 2017.

[73] Computer cluster, available online at: <http://hpc.ui.savba.sk/index.php?page=klaster>.

[74] R. Brambilla, F. Grilli, and L. Martini. Development of an edge-element model for AC loss computation of high-temperature superconductors. *Supercond. Sci. Technol.*, 20(1):16–24, 2007.

[75] E. H. Brandt and G. P. Mikitik. Vortex shaking and magnetic relaxation in superconductors. *Physica C*, 408-410:514–515, 2004.

[76] E. Pardo and F. Grilli. Numerical simulations of the angular dependence of magnetization ac losses: coated conductors, roebel cables and double pancake coils. *Supercond. Sci. Technol.*, 25:014008, 2012.

[77] F. Grilli, E. Pardo, A. Stenvall, D. N. Nguyen, W. Yuan, and F. Gömöry. Computation of losses in HTS under the action of varying magnetic fields and currents. *IEEE Trans. Appl. Supercond.*, 24(1):8200433, 2014.

[78] C.P. Bean. Magnetization of high-field superconductors. *Rev. Mod. Phys.*, 36(1):31–38, 1964.

[79] C. Navau, N. Del-Valle, and A. Sanchez. Macroscopic modeling of magnetization and levitation of hard type-II superconductors: The critical-state model. *IEEE Trans. Appl. Supercond.*, 23(1):8201023, 2013.

[80] M. Sander and F. Grilli. FEM-calculations on the frequency dependence of hysteretic losses in coated conductors. *J. Phys. Conference Series*, 234:022030, 2010. DOI: 10.1088/1742-6596/234/2/022030.

[81] K. P. Thakur, A. Raj, E. H. Brandt, J. Kvitkovic, and S. V. Pamidi. Frequency-dependent critical current and transport ac loss of superconductor strip and roebel cable. *Supercond. Sci. Technol.*, 24(065024), 2011. DOI: 10.1088/0953-2048/24/6/065024.

[82] K. P. Thakur, A. Raj, E. H. Brandt, and P. Sastry. Frequency dependent magnetization of superconductor strip. *Supercond. Sci. Technol.*, 24:045006, 2011. DOI: 10.1088/0953-2048/24/4/045006.

[83] M. Kapolka and E. Pardo. 3D modelling of macroscopic force-free effects in superconducting thin films and rectangular prisms. *Supercond. Sci. Technol.*, 32:054001, 2019.

[84] J.R. Clem, M. Weigand, J. H. Durrell, and A. M. Campbell. Theory and experiment testing flux-line cutting physics. *Supercond. Sci. Technol.*, 24:062002, 2011.

[85] J. H. Durrell, M. J. Hogg, F. Kahlmann, Z. H. Barber, M. G. Blamire, and J. E. Evetts. Critical current of $\text{YBa}_2\text{Cu}_3\text{O}_{7-\delta}$ low-angle grain boundaries. *Phys. Rev. Lett.*, 90(24), 2003. DOI: 10.1103/PhysRevLett.90.247006.

- [86] R. Herzog and J. E. Evetts. Low-temperature two-axis goniometer with accurate temperature control. Rev. of Sci. Instruments, 65:3574, 94.
- [87] T. D. Withnell, K. R. Schoppl, J. H. Durrell, and H. W. Weber. Effects of irradiation on vicinal YBCO thin films. IEEE Trans. Appl. Supercond., 19:3, 2009. DOI: 10.1109/TASC.2009.2019240.
- [88] M. Lao, J. Hecher, M. Sieger, P. Pahlke, M. Bauer R. Huhne, and M. Eisterer. Planar current anisotropy and field dependence of J_c in coated conductors assessed by scanning hall probe microscopy. Supercond. Sci. Technol., 30:024004, 2017.